Journal of The
Electrochemical Society

Physics-Based Analysis of Cell Imbalances and Aging in Lithium-Ion Battery Modules and Packs

To cite this article: Surya Mitra Ayalasomayajula *et al* 2025 *J. Electrochem. Soc.* **172** 080526

Journal of The Electrochemical Society, 2025 **172** 080526

Physics-Based Analysis of Cell Imbalances and Aging in Lithium-Ion Battery Modules and Packs

Surya Mitra Ayalasomayajula,[1,z] Yuliya Preger,[2] Jacob Mueller,[2] and Srikanth Allu[1,z]

[1] *Computational Sciences and Engineering Division, Oak Ridge National Lab, Oak Ridge, Tennessee 37830, United States of America*
[2] *Sandia National Labs, Albuquerque, New Mexico 87185, United States of America*

Lithium-ion battery (LIB) packs are a key solution for grid-scale energy storage, enabling grid resilience and supporting critical infrastructure. LIB modules and packs experience current imbalances and uneven cell aging due to various design and operational factors, and require a battery management system (BMS) to continuously monitor and control. In this context, a physics-based modeling framework for LIB modules and packs (`liionpack`) was enhanced to identify design and control strategies that minimize current imbalance and improve module/pack operation. Simulations of an 8-cell parallel-connected module demonstrate that reducing current imbalance leads to more uniform cell aging and improved module/pack-level degradation predictions. The analysis shows that current imbalance are affected by the electrical resistances. Terminal location significantly affects imbalance, with opposite-end terminal connections at intermediate branches minimizing the imbalance, and the pack circuit construction influences the accuracy of physics-based analysis at the pack scale. This framework enables design optimization of modules and packs through a fast and easy evaluation of pack performance and aging, and supports the development of aging-informed balancing strategies compatible with BMS implementation. Thereby, offering practical pathways to improve reliability and cycle life predictions in large-scale battery energy storage systems.

 [DOI: 10.1149/1945-7111/adf66f]

Manuscript submitted May 1, 2025; revised manuscript received July 3, 2025. Published August 20, 2025.

Lithium-ion batteries (LIBs) are gaining prominence for use in stationary energy storage systems for grid-scale applications,[1–3] since LIBs are well suited to stabilize power demand in modern energy systems and enable grid resilience,[4,5] through efficient short-term and long-term energy storage.[6] LIB battery modules and packs are developed by connecting cells in series and parallel to produce kWh- to MWh-scale battery energy storage systems (BESS),[7,8] which deliver high energy and power densities with low self-discharge while remaining cost-effective.[5,9] The LIB cells are connected in series to increase the total voltage output[10,11] and in parallel to increase the total charge capacity of the module/pack,[10] thus allowing flexible adjustment of the combination of series and parallel connections to meet specific application power and energy requirements.[8,12] Despite these advantages, LIBs are significantly affected by operating conditions, thermal fluctuations within BESS,[13,14] and the aging of individual cells.[14–16] Therefore, BESS must be consistently monitored through a battery management system (BMS) that accurately assesses the individual LIB state of charge (SOC), state of health (SOH), and temperature to maintain safe operation and improve performance and lifespan.[5,7]

A multitude of factors affect module and pack performance and aging.[17] On the cell level, differences in chemistries[18] and cell-to-cell variability[19] in internal resistances,[20] heat transfer coefficients, and charge capacities[21] play key roles. At the module and pack levels, connection resistances, electrical circuit design, thermal management, and operating conditions[22–26] substantially affect performance and aging. Imbalances within modules and packs can be minimized by efficient management of cells, achievable through various balancing strategies.[27–29] These balancing methods, along with appropriate control algorithms,[30] are used within BMS architectures.[31] Current imbalances within cells from different parallel branches are a key phenomenon that causes non-uniform aging and temperature gradients, posing challenges for the health and safety of modules and packs.[32,33] Therefore, understanding the factors that drive imbalance at the cell, module, and pack levels[5] is critical to improving module/pack design and developing model-informed, aging-aware BMS strategies that further enhance reliability and longevity.

In this regard, busbar interconnect resistance is one of the key factors affecting current imbalance in lithium-ion battery modules and packs, especially those with parallel connections. Wu et al.[25] utilized a pseudo two-dimensional (P2D) electrochemical-thermal model and demonstrated that even small busbar interconnect resistances between parallel branches cause current imbalances, leading to inhomogeneity in cell SOCs, temperatures, and impedances within the pack. They further showed a linear increase in imbalance as the number of cells in parallel increased, and a logarithmic increase in imbalance as the busbar resistance rose, with cells close to terminal connections experiencing the highest currents. Rumpf et al.[34] used a P2D model coupled with a lumped thermal model to simulate battery modules, showing that busbar resistances and symmetric cell connections significantly impact module performance. Ren et al.[35] employed a thermally coupled single particle model with electrolyte (TSPMe) to investigate the effects of thermal interactions and busbar interconnect resistance in a 30-cell parallel module, finding that even a 0.1 mΩ resistance caused current imbalances up to 9% during discharge, with cells near the load terminal receiving 65% higher currents, thereby increasing their risk of lithium plating and degradation. Recently, Piombo et al.[36] utilized experiments and a machine learning study to identify module-level factors influencing current imbalance, confirming that increasing busbar interconnect resistance was the most significant contributor among factors tested.

Beyond interconnect resistance, intrinsic cell-to-cell variability in internal resistance, capacity, thermal properties, electrode chemistry, and electrochemical kinetics also drives imbalance and heterogeneous aging. Gogoana et al.[20] showed that a 20% variation in internal resistance could cause a 40% reduction in module life, with some cells degrading faster due to disproportionate current draw. Bruen and Marco[10] employed an equivalent circuit model (ECM) to show that small deviations in resistance and capacity led to substantial skewing of thermal and electrochemical responses, increasing thermal stress and accelerating degradation. Luca et al.[33] experimentally investigated imbalance in an 8p1s module using Hall-effect sensors, confirming that lower-impedance cells consistently carried more current and aged faster. Piombo et al.[36] also demonstrated that using aged cells or cells with different chemistries increased imbalance due to variation in internal properties. Reiter et al.,[37] demonstrated methods to study cell-to-cell variations to determine the capacity and resistance deviation for cells in series topology.

[z]E-mail: ayalasomayas@ornl.gov; allus@ornl.gov

Thermal gradients within battery modules and packs further exacerbate imbalance and degradation heterogeneity. Liu et al.[32] used an experimentally validated thermally coupled single-particle model (TSPM) to show that elevated thermal gradients and higher C-rates amplify current imbalances and accelerate degradation mechanisms such as solid electrolyte interphase (SEI) growth. Ren et al.[35] highlighted that even when cell initial conditions are near identical, non-uniform temperature distributions increase imbalance and degradation variation, particularly when interconnect resistances are low. These results emphasize that uniform thermal management is crucial to achieving balanced module operation. Reniers et al.,[38] utilized a single particle model coupled with degradation kinetics to study a MWh scale battery system, highlighted that variations in the degradation rate of individual cells strongly influence the evolution of cell-to-cell variations over the system lifetime, while the thermal management critically impacts the pack life.

Moreover, terminal connection topology also influences current imbalance. Kim et al.[39] used an equivalent circuit model coupled with thermal analysis and modified nodal analysis to demonstrate that positioning terminals at opposite ends of a module rather than the same end, reduced current imbalance by 61.5%. Their findings showed that busbar induced voltage drops shift effective branch impedances, altering current distributions. Vikrant et al.[40] modeled the performance and aging of a 400p125s megapack using a degradation coupled single particle model, demonstrating that cells closer to load terminals experience accelerated degradation and that degradation inhomogeneity worsens with cycling. Recently, Preger et al.[41] have experimentally shown various design choices such as series or parallel first module configurations can significantly impact the performance specifically energy throughput, voltage divergence, and current imbalances. These results collectively highlight the need to optimize module and pack electrical layouts to mitigate degradation heterogeneity caused by imbalances.

Although prior experimental and simulation studies have investigated the effects of individual design factors, most modeling approaches either employ simplified equivalent circuit models at the cell level or are restricted to specific module sizes and configurations. Furthermore, experimental approaches require significant time and resources to capture module and pack aging dynamics. In this work, starting from experimentally validated single-cell and module simulations, we present a generalized, scalable physics-based modeling framework that extends from single cells to full packs while maintaining physical accuracy. We leverage the open-source `liionpack` framework,[42] built on single-cell electrochemical-thermal models, and modify it to analyze module and pack designs, balancing strategies, and degradation phenomena. This approach not only reproduces key trends reported in the literature but also enables predictive optimization of pack construction and aging-aware BMS design. Since current imbalance amplifies heterogeneity in cell aging, thus increasing uncertainty in lifetime prediction, physics-based design and control become essential for ensuring the performance, safety, and longevity of grid-scale battery energy storage systems. The developed framework offers a practical and scalable solution toward achieving these goals.

Methods

Module/pack simulations were performed using the open-source `liionpack` framework,[42] which solves physics-based models for each individual cell, while simultaneously updating the electrical currents in circuit branches at each time instance. Cell behavior was modeled using a Single Particle Model with electrolyte (SPMe),[43,44] implemented through the PyBaMM framework.[43] The SPMe model extends the single particle model by incorporating lithium transport in the electrolyte phase, thereby improving accuracy similar to a P2D model while being computationally efficient.[44] This enables scalable simulation of full battery modules and packs while maintaining physically realistic behavior at the cell level.

In the SPMe model, a representative spherical particle is considered within each electrode to represent the solid phase, and the diffusion equation is solved for lithium concentration in the solid phase. A volume-averaged diffusion equation is solved in the electrolyte phase of the electrodes and separator to account for lithium transport, while the terminal voltage is obtained through a simplified algebraic expression based on volume-averaged potentials. A lumped thermal model is used to compute cell temperature. The degradation mechanisms: solid electrolyte interphase (SEI) growth and porosity change due to SEI, lithium plating, and stress-induced loss of active material are incorporated, although no explicit coupling between degradation modes is considered. A detailed derivation of the model Eqs. are provided by Marquis et al.,[44] and further implementation details are available within the PyBaMM documentation.[45]

At the module/pack scale, the circuit is specified in a netlist format,[42,a] including all relevant nodes and circuit elements. The cell model parameters are provided in PyBaMM format within liionpack. The liionpack code updates the cell currents at each time step using the Modified Nodal Analysis algorithm,[47] wherein cell voltages are used to solve for the currents, which are then used in the subsequent step to solve the SPMe model for each cell and update the voltages. This iterative process continues until an end condition is met, such as voltage limits, end of life, or the end of a cycling protocol. Detailed information on the liionpack workflow is provided by Tranter et al.[42]

Current work utilized `liionpack` v0.4.0 and `PyBaMM` v24.9. Several extensions were made to liionpack to enable flexible pack-level simulations: (1) inclusion of inductive and capacitive elements in circuits, which are useful for representation of a BMS; (2) hierarchical construction of pack architectures from cells to modules to pack, offers an easy and efficient method to create large scale battery packs from simple commands; and (3) implementation of a balancing algorithm based on dynamic adjustment of series resistances. These modifications facilitate flexible construction of pack and module circuits, and enable multiscale analysis of cell, module, and pack performance and aging, demonstrating the framework's adaptability for BMS control implementation The use of a physics-based model at the cell level ensures physical consistency across module and pack scales.

Physics-based model parameters.—The experimental module utilized 3 Ah 18650 LGHg2 cells (see Section 3 for experimental details). Since `liionpack` employs SPMe single-cell parameters, cycling data from near-pristine 3 Ah 18650 LGHG2 cells was used to optimize the model. These parameters, excluding degradation effects, were identified using early stage cycling data when aging was considered negligible. As a detailed experimental characterization following the methodology of Chen et al.[48] was unavailable, the number of parameters optimized was reduced based on insights from existing literature.[49–51] The open-circuit voltage profiles for the electrode materials were taken from.[48]

On the single-cell scale, the "Okane2022" parameter set available in PyBaMM[52] was modified. Most of the relevant parameters from literature were adopted, and the electrode maximum lithium concentrations were constrained using electrode capacity and porosity relationships:

$$(x_{a,100} - x_{a,0}) c_{s,a}^{\max} V_a \epsilon_{a,\mathrm{act}} \mathcal{F} = C_a \times 3600, \quad [1]$$

$$(y_{c,100} - y_{c,0}) c_{s,c}^{\max} V_c \epsilon_{c,\mathrm{act}} \mathcal{F} = C_c \times 3600, \quad [2]$$

where $\mathcal{F}$ is Faraday's constant, $x_{a,100}$, $x_{a,0}$, $y_{c,100}$, $y_{c,0}$ are anode/cathode stoichiometry ratios at 100% and 0% SOC, $c_{s,a}^{\max}$, $c_{s,c}^{\max}$ are maximum lithium concentrations, V_a, V_c are electrode volumes, C_a, C_c are electrode capacities, and $\epsilon_{a,\mathrm{act}}$, $\epsilon_{c,\mathrm{act}}$ are active volume fractions. Using fitted porosity values from,[50] stoichiometry ratios and electrode volumes from,[49] and the electrode capacity range suggested by,[49,51] a corresponding range of feasible maximum concentrations was estimated using: $x_{a,100} = 0.90$, $x_{a,0} = 0.052$, $y_{c,100} = 0.89$, $y_{c,0} = 0.27$,

[a] A netlist comprises a list of all circuit elements and their respective positive and negative node numbers in columns. It can be constructed graphically using LTspice,[46] see Fig. 3a, or through a set of commands within the framework.

Table I. Optimized parameters for single cell SPMe model in PyBaMM.

Parameter Definition	Units	Optimized value	Initial value	Bounds [lower,upper]	Prior distribution
Maximum lithium concentration in negative electrode ($c_{s,a}^{\max}$)	mol/m^3	33115	33700	[32610, 34859]	Uniform
Maximum lithium concentration in positive electrode ($c_{s,c}^{\max}$)	mol/m^3	45175	44732	[43241, 46223]	Uniform
Negative particle radius ($r_{p,a}$)	m	9.6e-06	9.0e-06	[6e-6, 10e-6]	Gaussian (mean = 8e-06, variance = 3e-06)
Positive particle radius ($r_{p,c}$)	m	1.49e-06	2.0e-06	[1e-6 , 5e-6]	Gaussian (mean = 4.5e-06, variance = 2.5e-06)

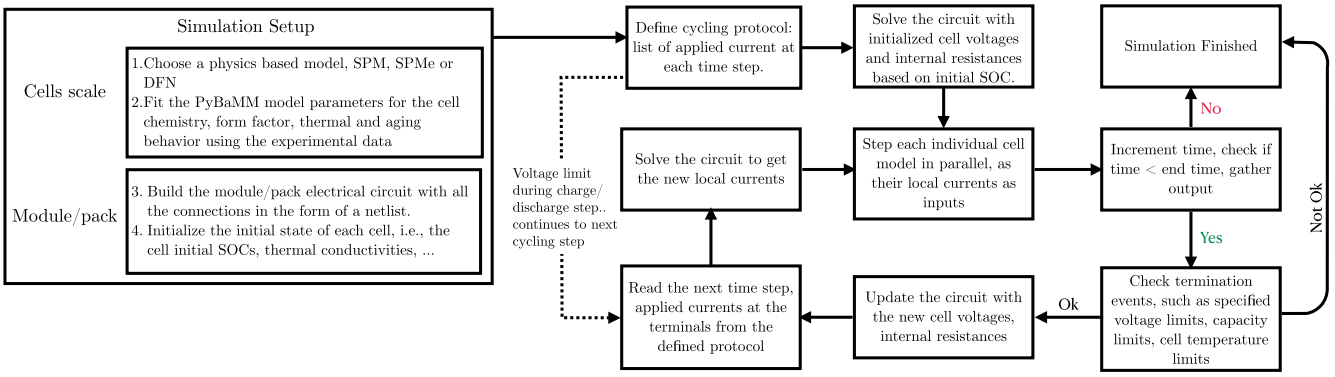

Figure 1. A schematic of the applied method highlighting the simulation steps and an updated liionpack workflow replicated from.[42]

$V_a = 0.060 \times 1.85 \times 5 \times 10^{-5} m^3$, $V_c = 0.060 \times 1.85 \times 4.5 \times 10^{-5} m^3$, $\epsilon_{a,\text{act}} = 0.705$, $\epsilon_{c,\text{act}} = 0.808$, $C_a = [2.9, 3.1]$, and $C_c = [2.9, 3.1]$.

Degradation parameters were adopted without modification,[b] as the electrode materials closely resemble those of the LG M50 cells. The following degradation mechanisms were included: SEI growth, irreversible lithium plating, and stress driven loss of active material, consistent with those reported for the LGHG2 cells in this work.[53] See Table A.1 in Appendix A for the full list of PyBaMM parameters updated from the "Okane2022" parameter set.

The modified "Okane2022" parameter set, comprising both literature-sourced and pre-existing PyBaMM parameters was used as the baseline for optimization. Cells were initialized at 100% SOC and subjected to the same C/2 constant current (CC) cycling protocol with voltage cutoffs as described in Section 3. Optimization was performed using the PyBOP framework[54,55] to estimate the maximum lithium concentrations and the representative particle radii for each electrode. The Covariance Matrix Adaptation Evolution Strategy (CMA-ES) algorithm was employed, using the root mean squared error (RMSE) between simulated and experimental voltage profiles as the objective function. Table I, highlight the optimized parameters and details.

For validating the optimized results, cells were initialized at 100% state of charge (SOC), and subjected to similar constant current (CC) charge/discharge cycling at C/2 and up to 3C rates, with voltage cutoffs matching the experimental protocol.

On the module scale, as liionpack relies on PyBaMM for cell modeling, the module circuits were constructed using a netlist format, and the optimized SPMe parameters were assigned to each cell. Experimental cycling protocols were input in PyBaMM compatible format. For the module experimental validation, the experimental circuit was replicated, the initial SOC of all the cells was adjusted to 0.22, the cell cut off voltages match the experimental setup and the module was cycled similar to the experiments. Throughout the rest of the analysis, the module circuits were constructed using different resistance values, and all cells were initialized at 100% SOC and 298.15 K (25 °C) at the start of the simulations, unless otherwise specified. In all the module simulations, the cells start from same initial conditions, such as capacities, SOC and internal resistances. No external thermal management (cooling) was modeled beyond cell-level lumped thermal dynamics, since liionpack lacks cell-to-cell thermal interaction model. A schematic of the liionpack modeling workflow is shown in Fig. 1.

All simulations were carried out on a 16 GB Apple M2 machine, standard solver tolerances from PyBaMM were used, with a relative tolerance of 10^{-6} and absolute tolerance of 10^{-8}. Typical wall times were approximately 1 second per single cell cycle and approximately 50 seconds per full module cycle.

Experimental Setup and Data Generation

The data used for single cell SPMe model parameter estimation was previously reported cycling data for 3 Ah 18650 LG Chem HG2 NMC811 cells. The cells were cycled at 0–100% SOC (2–4.2 V according to the manufacturer's specifications), at a charge rate of 0.5C and discharge rates of 0.5C, 1C, 2C, and 3C. The nominal capacity of the cell was used as the basis for calculating C-rates. Cycle aging was carried out in a temperature-controlled chamber at 25 °C. The full experimental configuration is detailed in the original publication.[56] The raw time series data were downloaded from Battery Archive.[57]

The module data used, was previously reported cycling data for an 8P-1S module composed of the same type of NMC cell.[41,58] The individual cells were instrumented with temperature, voltage, and current sensors. The current was measured using closed-loop Hall effect sensors (LEM LTS-15NP), which provide high sensing accuracy with less than 1 mΩ of insertion resistance. The module cycling protocol consisted of constant current charge and discharge at 0.5C (12 A, based on the module's total nominal capacity of 24 Ah) with thirty-minute rests in between. A charge or discharge step was considered complete once any cell in the module reached

[b]While the degradation study could benefit from further optimization using long-term data for LGHG2 cells, the available parameters were sufficient to capture imbalance-driven degradation trends in this study.

the voltage limit (4.1 V during charge or 2.5 V at discharge). The module did not have a battery management system or active/passive balancing. For safety, the cycling program had abort limits based on cell-level voltage, current, and temperature (from manufacturer's specifications[59]) and the module-level voltage and current.

Results and Discussion

Experimental validation.—Figure 2, highlights the comparison of the single cell simulations against experimental data. The optimized SPMe model parameters yield accurate results at C/2 charge and discharge, as seen in Fig. 2a. The cell relaxation behavior predicted by SPMe model after discharge for 600s, showed a slight mismatch with the experiments due to simplification employed for diffusion in the solid phase, instead a many particle model (MPM) model keeping the average particle radius the same with adjusted particle size distribution parameters was able to capture the relaxation behavior accurately, but MPM model takes 10× more computation time and liionpack framework currently support SPM and SPMe models with degradation effects on a single cell. Despite this, the SPMe model predicted the discharge behavior of cells at 1C with 97% accuracy, as seen in Fig. 2b. Overall, the SPMe model was able to predict the single cell discharge behavior close to experiments with more than 89% accuracy for C-rates ranging from 0.5C to 3C, see Fig. B·1 from Appendix B.

The module-level simulation compared against the experiments are highlighted in Fig. 3. The module simulation results highlight cell current distributions similar to experiments. However, the current imbalance of cells shows a different trend from experiments, due to a mismatch of the individual cell internal states prior to the module cycling experiments, as observed from cycling the cells before plugging into the module see Fig. B·2, from Appendix B, implying that each cell in the module starts from a different initial condition in module experiments. Nevertheless, given the single cell model was optimized against experiments and assuming all cells begin with the same initial conditions, the module simulations align with the current distribution range observed in experiments, i.e., $\frac{(I_{\max}-I_{\min})_{\text{sim}}}{(I_{\max}-I_{\min})_{\text{exp}}}$ is less than 5%. This suggests that the module-level physics-based modeling approach is effective, since the single cell model and modified nodal analysis are physically accurate, the accuracy of module simulations ultimately depends on the initial conditions for the cells before starting the simulation. Therefore, despite mismatches between the simulation and experimental data, module level physics based model is effective for analysis of LIB modules.

Module/pack current balancing strategies.—The module simulations in liionpack provide an accurate representation of experimental results, given an optimized single cell model parameters, representative module circuit construction, and right initial conditions for individual cells. Thus, current balancing strategies were explored using the liionpack framework, with the optimized single cell parameters, assuming all the cells have identical initial conditions, and utilizing a simplified circuit shown in Fig. 4 for the analysis.

Figure 4, shows the circuit diagram of an 8p1s module considered to test the module/pack balancing strategies. Here, R_{bp} and R_{bn} represent the busbars connected on the positive and negative ends of the parallel branch. R_i is the battery internal resistance, and R_{tp} and R_{tn} are the resistances at positive and negative terminal connections. The nodes at the ends of a parallel branch are denoted with the branch number followed by p for positive and n for negative end, such as 1p and 1n. All other resistances in series within a parallel branch are lumped as a single connector resistance R_c for simplification since currents imbalances are looked at[c]. Further, the cells are denoted as voltage sources V and the overall module charge/discharge currents are denoted by I_0.

The 8p1s module in Fig. 4, the uniform busbar resistances $R_b = 1\,\text{m}\Omega$, uniform connector resistances $R_c = 10\,\text{m}\Omega$, terminal resistances $R_t = 10\,\mu\Omega$, were considered, [17] while the cell internal resistances was initialized close to $R_i = 0.4\,\text{m}\Omega$. The value for the busbar resistance was arbitrarily chosen based on the practical range of connection resistance values being in the order of 1 mΩ,,[17] similarly the total connector resistance was selected to be 10 mΩ, given the values from experiments in Fig. 3a are on the same order, and the terminal resistance values were assumed to be a low value. The cell internal resistance values were initialized to an acceptable value.[48]

Figure 5a shows that cells in the 8p1s module experience current imbalance, in this case the expected ideal current in each cell is 3A for discharge, 0A for rest and −3A for charge, but cells closer to the terminals experience nearly twice the average, while the cells farther from the terminals experience lower currents than the ideal value. This current imbalance is quantified using a RMS deviation metric, $\text{RMS}_{\text{i}} = \left(\sqrt{\Sigma_i^N\left(\frac{y_i - y_m}{y_m}\right)^2/N}\right) \times 100$, here y_i is the value at a time instant i and y_m is the expected value. The deviation of the currents for individual cells was measured with respect to the expected current values, in agreement with most studies. Figure 5b, shows that cells age differently due to current imbalance, which could lead to an uncertainty in module life and aging predictions in practical applications. Especially, for the constant current cycling of the module, cells that experience high currents have an accelerated capacity loss due to degradation mechanisms, such as SEI, lithium plating and active material loss due to electrode particle fracture.[60] Moreover, during long-term cycling, cell-to-cell heterogeneity can cause certain cells to reach end-of-life earlier than others, even though the module as a whole may still appear operational. This mismatch in aging can pose significant safety risks to the entire module. For instance, as shown in Fig. C.1 (see Appendix C), the internal resistance of some cells increases steadily with continued cycling, a trend that may elevate the risk of thermal runaway in severely aged cells. Further observed in Fig. C.2 (see Appendix C), some degradation modes could be more actively accelerating aging. Therefore, minimizing current imbalances within the module could improve the module/pack cycle life predictions by minimizing heterogeneous aging of cells.

A conceptual balancing strategy was applied to a module, inorder to demonstrate the modeling framework's capability to incorporate BMS control algorithms. Specifically, the connector resistance in series to the cells was adjusted as a variable resistance based on the difference in cell current from the mean expected current at each time step. The connector resistance was chosen since: (1) a series resistance to cells dissipates the power received by the parallel branch; (2) all resistive elements connected in series with the cells can be lumped into a single equivalent connector resistance without affecting DC current paths or simulation results, simplifying the module circuit without compromising accuracy; (3) switching of resistors is a widely demonstrated balancing method.[27,29,31] Although active balancing is typically implemented at the module level due to cost and complexity constraints, a cell-level strategy was used here as a conceptual tool to study the impact of current imbalance. Nonetheless, the proposed approach is scalable across modules in a pack, enabled by the framework's ability to implement control algorithms through circuit-level adjustments. This method of using resistive elements could cause the heating of the circuit elements since resistances dissipate excess power in the parallel branch. Despite the practicality of the BMS algorithm, the primary aim of this method is to showcase the effects of minimizing current imbalances on the aging behavior and predictions and demonstrate the capability of the framework to implement BMS control algorithms.

Figure 6, shows the effects of minimizing current imbalances within a module, using the conceptual strategy. For the 8p1s module circuit shown in Fig. 4, the current imbalance could be minimized by actively adjusting the connector resistances, as seen in Fig. C.3, from Appendix C, here the cell currents are balanced within the first five cycles, also observed as the connector resistances adjust toward constant values. The results highlight that lower current imbalances

[c]Since all the elements connected in series experience same DC currents, the simplification of having one total connector resistance do not alter the current imbalance results from simulations.

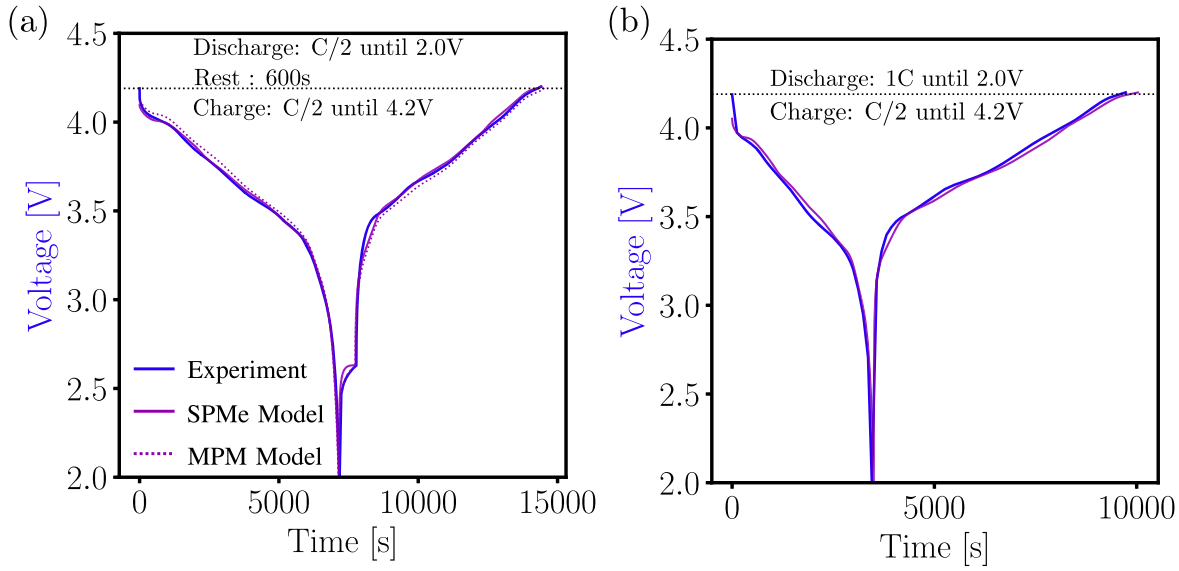

Figure 2. Comparison of single cell simulations against experimental data. Inset (a), shows the comparison of simulated results for a single cell against experimental data at C/2 discharge until 2.0 V followed by 600 seconds of rest and C/2 charge until 4.2 V. The SPMe model parameters were optimized for C/2 discharge, matched the experiments with an R^2 score of 0.99. Inset (b), shows the testing of optimized single cell parameters at 1C discharge followed by a C/2 recharge, wherein the simulations matched the experiments with an R^2 score of 0.97. Therefore, the optimized parameter set for the single cell was able to predict the cycling behavior of cells at near pristine conditions with negligible degradation effects.

allow all the cells to degrade uniformly as seen in Fig. 6b, and Table II, quantifies the percentage change in charge capacity loss of cells after balancing, shows the cell aging variation without any current balance was nearly ∼7% at 1200hrs for the cycling currents and the degradation parameter set utilized. The degradation heterogeneity within the cells is further amplified when higher cycling currents are applied, and/or more cells are connected in parallel, since current imbalances are amplified in both the cases,[25,32,35] see Fig. D·1 from Appendix D. A comparison of module capacities, as shown in Fig. 6c, highlights that although the improvement with active balancing is 2.38% on average under the tested operating conditions and module configuration, the module capacity closely matches that of the individual cells. This suggests improved predictability of module aging after balancing. In contrast, heterogeneous aging of cells within a module can significantly affect the accuracy of long-term aging predictions. Overall, minimizing current imbalances promotes uniform aging across individual cells and enhances the reliability of module-level degradation forecasts. Furthermore, developing efficient strategies to manage these imbalances can support the design of aging-informed BMS.

Impact of resistive elements in a module.—Figure 7a, shows the effect of changing the busbar resistance (R_{bn}, R_{bp}) uniformly in the module, suggests lower busbar resistances are preferable to minimize the imbalance, in agreement with Luca et al.,[25,33] because the busbars cause a difference in potential across each parallel branch that leads to different currents in each branch. This is evident when the busbar resistance tends to zero there is zero current imbalance among the cells. While a zero busbar resistance is impractical, for a given busbar resistance, uniformly increasing the connector resistances R_c minimizes the current imbalance, as seen in Fig. 7b. Increase in connector resistance increases the potential drop in series to the cell that acts as a damper to the oscillations in the currents by dissipating energy as heating of resistors. Although the current imbalance is minimized as the series resistance increases, beyond a certain value heating of the module could be a potential concern.[d] Figure 7c, shows the effects of adding more cells in series in a parallel branch of the module given fixed uniform busbar and connector resistances. Current imbalance in the parallel branches minimizes as cells are added in series, similar to liu et al.,[32] since each cell has an impedance that has a similar effect of increasing the connector resistance, and there is no significant loss of energy due to dissipation, but failure of a cell in series of a branch can increase impedance and cause thermal runaway issues. Nonetheless, this analysis suggests carefully adjusting the resistances, i.e., increasing resistances in series within a parallel branch or reducing the busbar resistances, minimize current imbalance and improve module/pack performance.

Effects of terminal connections on current imbalances.—Figure 8, shows that choice of terminals is essential to minimize current imbalance when all the resistances are fixed, here the busbar resistances $R_b = 1$ mΩ, connector resistances $R_c = 10$ mΩ, terminal resistances $R_t = 10$ μΩ. For each module size, within the heat maps, the location of positive terminal on a parallel branch is represented as the columns and the negative terminal on the parallel branch is represented as rows, as such a combination of a particular (column, row) numbers represent a unique terminal connection, for example from Fig. 4 the terminals are connected on (1p,1n) common-end configuration, here represented from the first row and first column on Fig. 8c. The effects of different terminal combinations for different module sizes were observed, as heat maps of RMS average values. The RMS average is calculated as the mean of RMS deviations, RMS_i, in all parallel branches i.e., $\mathrm{RMS_{avg}} = \sum_i^N \mathrm{RMS}_i/N$, where N is the number of parallel branches. Here, high RMS average implies large imbalance in currents, therefore terminal combinations with lower RMS average values are preferable for low current imbalances. The common-end configurations such as (1p,1n) or (8p,8n), lead to the highest imbalance in all module sizes tested, while opposite-end configurations showed less current imbalance in comparison to the common-end configurations, in agreement with Kim et al.[39] For the module with $3 < n \leqslant 8$ parallel branches the terminals at second and n-1 branches minimize the current imbalance, for example in a 8p1s module, Fig. 8c, terminal locations at (2n,7p) and (2p,7n) minimize the imbalance, and as the number of parallel branches in a module increase the optimal terminal locations move to (3,n-2), (4,n-3) and (5,n-4) as observed in Figs. 8d–8f. This is because, the terminal locations determine the currents drawn by each branch, for example, when the terminals are connected at opposite-end configurations at intermediate locations, the effective impedances observed by the parallel branches are minimized while

[d]Simulations highlighting cell-to-cell thermal interactions are needed to further study module heating effects and thermal hot spot formations.

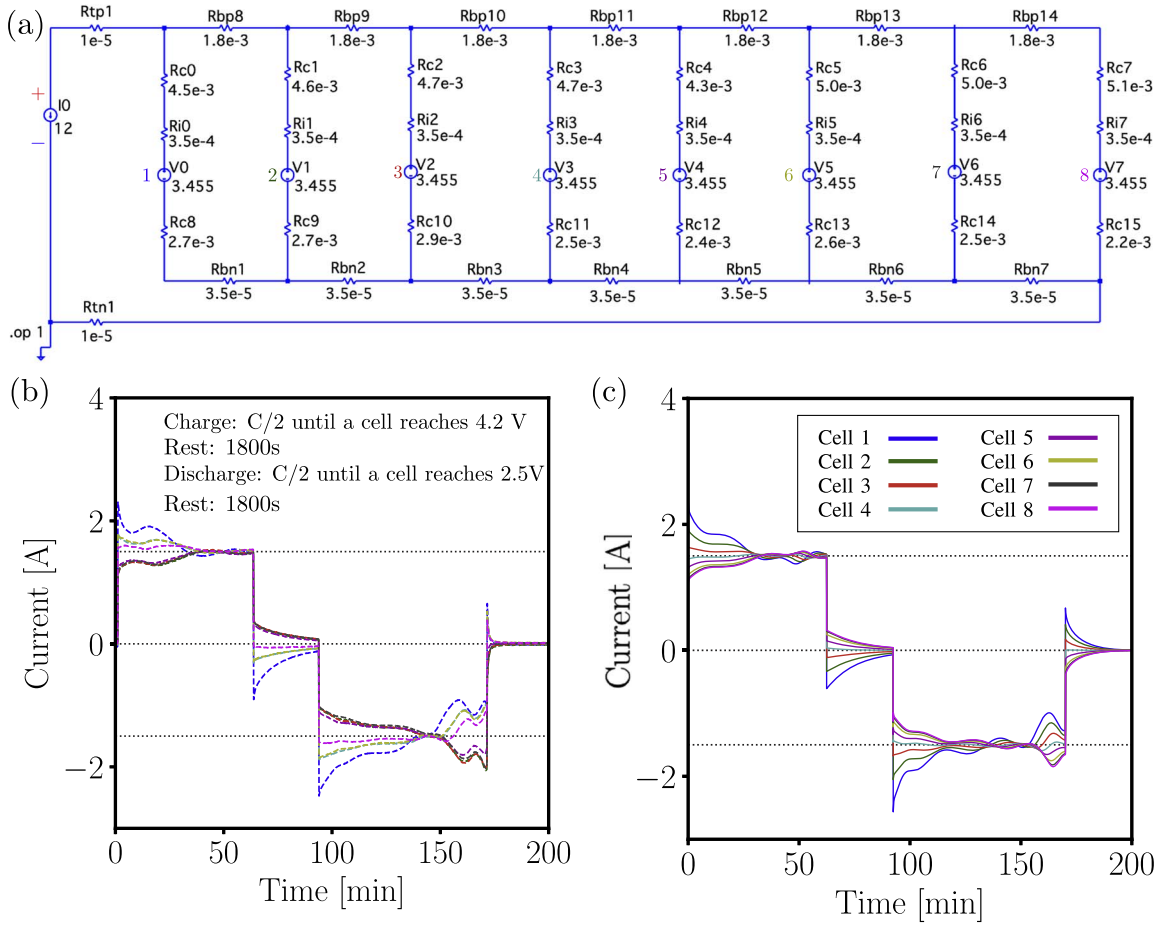

Figure 3. Module physics based model validation against experiments. Inset (a) shows the schematic of the 8p1s module circuit used for the experiments, here all resistance values are in Ohms Ω, Rbn and Rbp represent the negative and positive busbars interconnect resistances, Rc are the connector resistances, Ri are the assumed initial values of cell internal resistance, Rtp and Rtn are the positive and negative terminal resistances, V represents the individual cell starting voltages in volts *V*, and I0 is the applied module currents in amperes *A*. Insets (b) show the experimental and inset (c) shows the simulation results for the individual cell currents within the module shown in inset (a). The module simulations capture the ranges of cell current imbalance, but individual cell currents differ from experiments mainly due to the cells in the experimental module start from slightly different initial conditions, see Fig. B.2, from Appendix B, but all the cells in the module are considered identical for the simulation.

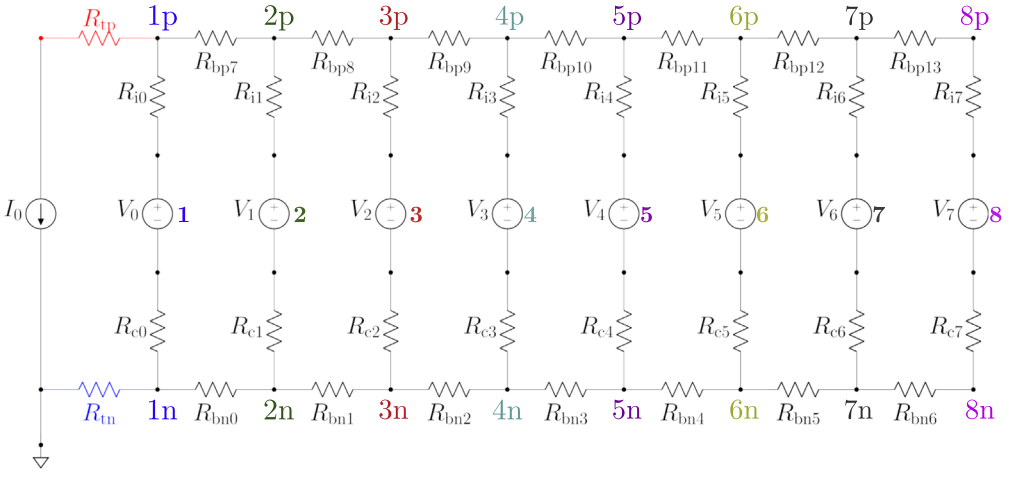

Figure 4. Circuit schematic of an 8p1s battery module, highlighting the different circuit elements such as busbars (R_{bn},R_{bp}), total connector (R_c) resistance, terminal connection resistances (R_{tn},R_{tp}), cell voltages *V* and module input current I_0.Each parallel branch has a positive and negative nodes such as 1p, 1n to further simplify analysis of module/pack balancing strategies with terminal connections.

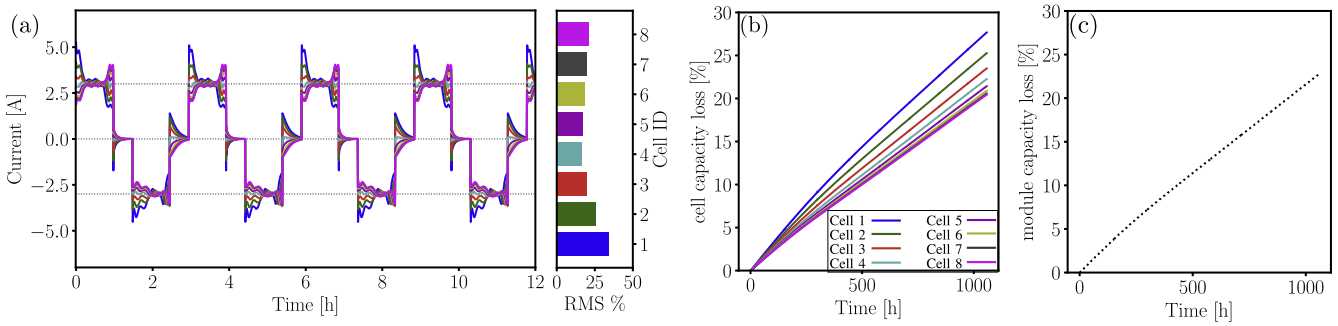

Figure 5. Heterogeneity in degradation of individual cells in the 8p1s battery module from Fig. 4, given all the cells are identical and start from the same initial conditions. Inset (a) shows cells currents experienced when the module is cycled at 1C discharge (24A) for 3600seconds followed by rest for 1800seconds, 1C charge for 3600seconds and rest for 1800seconds, when the cells initial SOC is 100%. The RMS metric highlights the current imbalance in cells, suggesting that the cells in a module experience currents different from the expected 1C $\sim$ 3A. Inset (b), shows the percentage loss of cell charge capacity due to degradation mechanisms such as SEI and porosity changes due to SEI, lithium plating, active material loss on each individual cell, and inset (c), shows the module charge capacity loss, when cycled 400 times ($\sim$1200 hr). The cells age differently in battery modules and packs due to the imbalance in the currents during charging and discharging, thereby causing the module/ pack to age faster than expected.

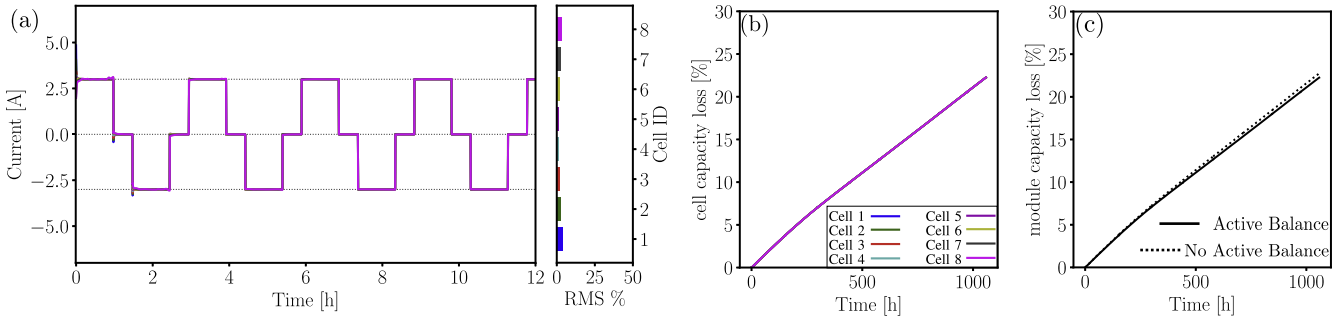

Figure 6. Actively balancing cell currents in the module to minimize aging heterogeneity. Inset (a), highlight the currents in the cells when the 8p1s module was cycled at the same conditions as Fig. 5, but with a series connector resistance that varies according to the branch currents, which minimizes the current imbalance. Inset (b), shows the percentage loss of individual cell charge capacity after balancing, here all the cell exhibit similar aging behavior, and inset (c), highlights the module charge capacity loss with and without the balancing strategy, improve module life by 2.38% on average for the tested conditions. Minimizing imbalance minimizes the heterogeneity in cell aging and improve the module performance predictions and provide control strategies that aid in development of an aging aware BMS.

Table II. Changes in the cell charge capacity loss after incorporating an active balancing strategy.

Cell ID	1	2	3	4	5	6	7	8
% improvement in cell capacity loss after the active balance	−26.61	−14.86	−5.828	0.68	5.05	7.87	9.56	10.35

−, negative implies a reduction in capacity loss after balancing i.e. improved aging of the cell.

also being uniform which lead to near uniform currents through the cells.[39] Although the heat maps are subjected to change when non-uniform resistances are used, different cells are used and/or the module/pack circuit changes i.e., has more cells in series per branch, the best possible terminal location could be identified easily through repeating the following analysis for any modules/packs.

Module to packs hierarchical construction.—Cells to module to pack hierarchical circuit construction was implemented in liionpack, enabling battery packs to be built from modules connected in series and parallel using simple commands. To examine the effects of construction hierarchy, two configurations with identical cell count, total capacity, voltage limits, and nominal power were compared: a pack of three 8p1s modules connected in series 3x(8p1s) (Fig. 9a) and a single 8p3s module pack (Fig. 9b). Both setups contain 24 cells, offer a capacity of 24 Ah, and operate within a voltage range of 6.0–12.6 V ±10 mV, and yield a total discharge energy of 244.8 Wh. Despite these similarities at the pack level, Fig. 9c shows that the cells in 3 × (8p1s) configuration exhibit greater current imbalance compared to the 8p3s configuration. This is because, in the 8p3s configuration, cells are connected in series within each parallel branch, and each cell shares the branch current with two other cells, which reduces the cell current imbalances, as also seen in Fig. 7c. In contrast, in the 3 × (8p1s) configuration, each cell is connected only in parallel, and series connections exist only at the module level, resulting in current imbalances similar to those observed in a standalone 8p1s module. Since, minimizing imbalances minimizes the aging heterogeneity among the cells, this means the pack in Fig. 9a is expected to experience more heterogeneity and high uncertainty of pack aging prediction, and an increased risk of failure, in comparison to the module in Fig. 9b, when cycled for long term. This shows that a correct representation of a module/pack circuit is essential for an accurate physics based analysis, i.e., although both the circuits here deliver the similar overall voltages, currents and capacities, they exhibit significant differences in the individual cell aging, and the overall module/pack aging predictability.

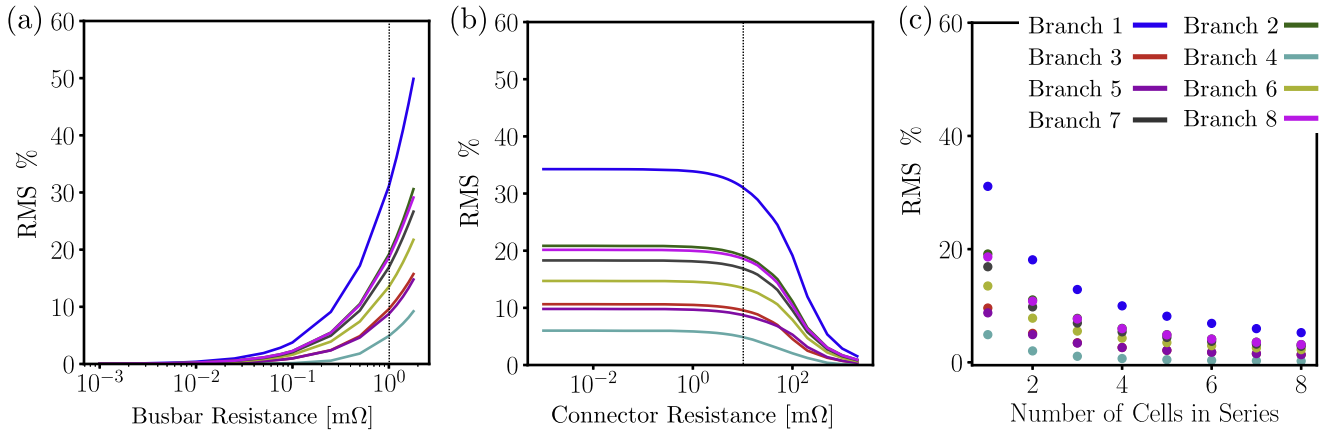

Figure 7. Impact of resistances in module construction. Inset (a), shows increasing busbar resistance uniformly, exponentially increases the imbalance of cell currents in the module, the vertical line highlights busbar resistance of 1 mΩ, while the connector resistances were maintained constant at 10 mΩ. Inset (b), shows uniformly increasing connector resistance in series to the cells minimize the current imbalance, while a uniform busbar resistance of 1 mΩ was maintained. Inset (c), highlights adding cells in series within a parallel branch also minimize the cell current imbalance, given all other resistances were maintained constant. Overall, the current imbalance in parallel connected cells could be minimized by reducing busbar resistance, or increasing the resistance in series in a parallel branch by increasing the connector resistance or adding more cells in series. Therefore, the module/pack design is optimized to minimize the current imbalances through appropriate choice of the circuit elements.

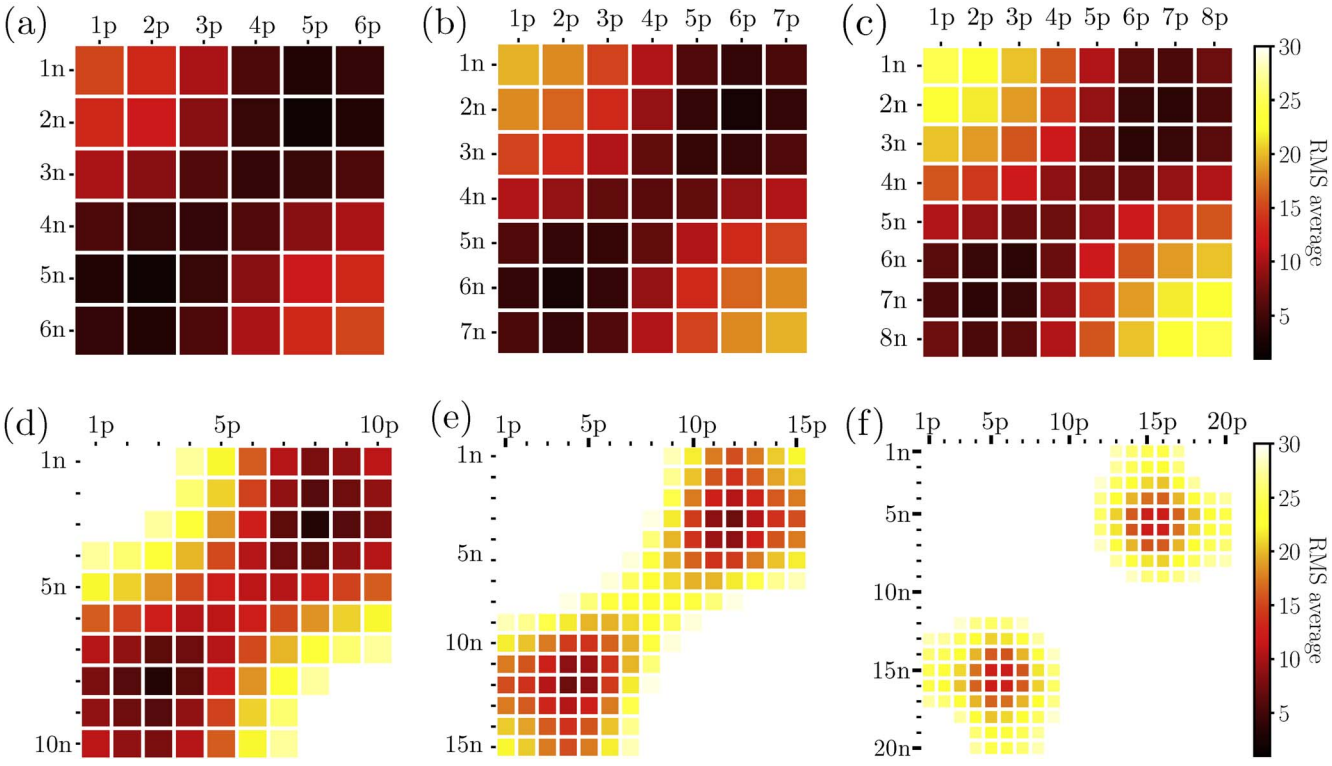

Figure 8. Effects of terminal location choice on cell current imbalance in parallel connected cells. Heat maps highlight the average RMS change of cells currents in the module at all possible terminal location combinations, where columns represent the positive terminal location, i.e., 1p means the positive terminal is connected to the positive end of the first branch, and the rows represent the negative terminal location, i.e., 1n means the negative terminal is connected to the negative end of the first parallel branch as seen from Fig. 4. Thus a given combination of a (column number,row number) such as (1p,1n), (1p,8n) or (2p,16n) represent a unique terminal connection. The heat maps for multiple module sizes are shown, (a) 6p1s module, (b) 7p1s module, (c) 8p1s module, (d) 10p1s module, (e) 15p1s module, (f) 20p1s module, where low RMS average implies a low current imbalance. The optimal terminal locations to minimize imbalance changes with the number of parallel connections, but in all cases the terminals connected to intermediate branches at an opposite-end configuration minimized imbalance.

Conclusions

A physics-based module/pack simulation framework, liionpack was extended for the analysis of factors affecting cell current imbalances and strategies to minimize imbalances. The framework was built on an electrochemical-thermal models for individual cells through PyBaMM, and coupled with a circuit-level modified nodal analysis to solve for branch currents at each time step. Experimental validation was carried out using single-cell data for LG HG2 NMC–graphite 3 Ah 18650 cells. The SPMe model, optimized with early-cycle data, showed strong agreement with experiments across a range of C-rates. For module-level simulations, the

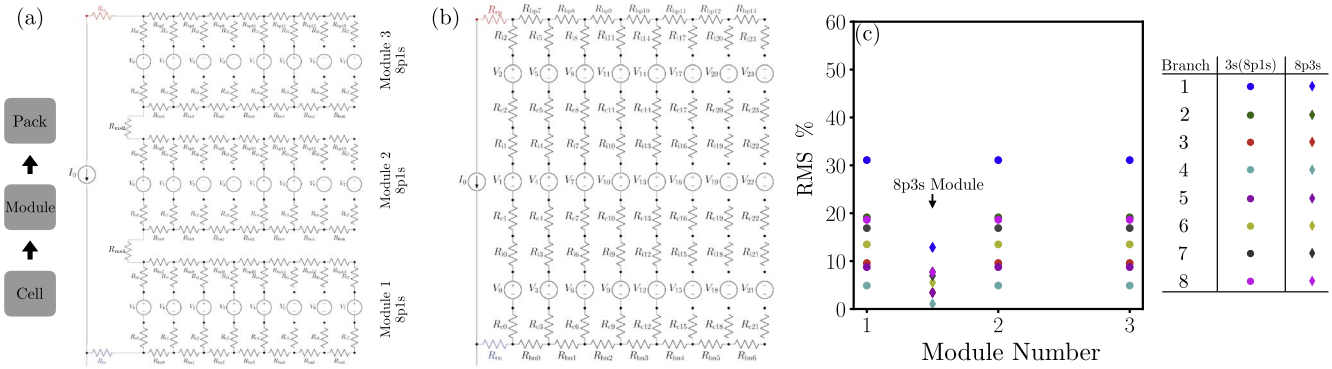

Figure 9. Current imbalance variations due to pack and module constructions. Inset (a), shows the schematic of a pack constructed from three 8p1s modules connected in series 3s(8p1s). Inset (b), shows the schematic of 8p3s module constructed by connecting 3 cells in series per parallel branch. Inset (c), highlights the current imbalance within cells in each module for the 3s(8p1s) pack and the cells in a 8p3s module. The battery pack circuit construction is important for analysis of cell currents and voltages and subsequent pack aging analysis.

framework reproduced the experimentally observed range of current imbalance, although exact cell-to-cell agreement was limited by unknown initial conditions in the experimental setup.

The results demonstrate that cell current imbalance is a critical driver of heterogeneous aging within battery modules, increasing uncertainty in cycle life predictions and degrading pack-level performance, in agreement with observations from literature. A systematic analysis revealed that design parameters, such as busbar resistance, connector resistance, number of cells in series, and terminal connection topology substantially affect current distributions. Balancing strategies were also explored within the modeling framework, including a conceptual algorithm that adjusts series connector resistances based on measured imbalances. This approach led to more uniform cell currents, reduced degradation variability, and an overall improvement in cycle life under tested conditions. These findings highlight that informed module/pack design and appropriate control strategies are essential for maintaining safety, longevity, and accurate performance estimation in large scale energy storage systems. Despite the physical implications and practical challenges, optimal strategies for construction and control of modules/packs is possible through the following framework and analysis.

While the current model successfully captures many physical trends necessary to improve module/pack design, performance and aging, several aspects require further development to enhance its predictive capability and practical relevance. For example, a more refined identification of degradation parameters using long-term aging experiments would improve accuracy in predicting cell-level capacity fade and performance loss. Further, incorporate models for cell-to-cell thermal interactions, as uneven heat distribution can compound imbalance and lead to localized degradation or safety concerns, and also the heating of the resistors need to be considered for more physically accurate thermal management. Additionally, there is potential to expand the framework with experimentally validated control algorithms for aging-aware balancing and thermal management, moving toward a more realistic simulation of a BMS. This includes integrating active/passive balancing strategies with thermal constraints and adaptive current control. Finally, improved methods for estimating initial cell conditions in experimental modules would help close the gap between model predictions and real-world performance, particularly for validating aging behavior over extended cycling.

Acknowledgments

This material is based upon work supported by the U.S. Department of Energy, Office of Electricity (OE), Energy Storage Division and was carried out at Oak Ridge National Laboratory under Contract No. DE-AC05-00OR22725 with UT-Battelle, LLC. Also, co-authors of this article are employees of National Technology & Engineering Solutions of Sandia, LLC under Contract No. DE-NA0003525 with the U.S. Department of Energy (DOE). The authors owns all right, title and interest in and to the article and are solely responsible for its contents. The United States Government retains and the publisher, by accepting the article for publication, acknowledges that the United States Government retains a non-exclusive, paid-up, irrevocable, world-wide license to publish or reproduce the published form of this manuscript, or allow others to do so, for United States Government purposes. The Department of Energy will provide public access to these results of federally sponsored research in accordance with the DOE Public Access Plan (http://energy.gov/downloads/doe-public-access-plan).

Appendix A: Single Particle Model with Electrolyte (SPMe) Parameters

Table A.I. List of parameters for single cell SPMe model in PyBaMM[a].

Parameter Definition	units	value	references
Ambient temperature	K	298.15	—
Cell cooling surface area	m^2	0.003676	49,50
Cell volume	m^3	1.654e-05	49,50
Total heat transfer coefficient	$W.\ m^{-2}\ K^{-1}$	9.0	50
Contact resistance	Ω	3.70e-04	49–51
Electrode height	m	0.060	59
Electrode width	m	1.85	49
Negative electrode initial stoichiometry at 100% SOC ($x_{a,100}$)	—	0.90	49
Positive electrode initial stoichiometry at 100% SOC ($x_{c,100}$)	—	0.27[a]	49
Initial concentration in negative electrode	mol/m^3	$x_{a,100}c_{s,a}^{\max}$	—
Initial concentration in positive electrode	mol/m^3	$x_{c,100}c_{s,c}^{\max}$	—
Nominal cell capacity	A.h	3.0	59
Open-circuit voltage at 0% SOC	V	2.0	59
Open-circuit voltage at 100% SOC	V	4.0	59
Negative electrode thickness	m	5.0e-05	49
Negative electrode Bruggeman coefficient (electrolyte)	—	1.5	50
Negative electrode active material volume fraction ($\epsilon_{a,act}$)	—	0.71	50
Negative electrode porosity (ϵ_a)	—	0.25	48,50
Negative current collector density	kg/m^3	8950.0	50
Negative current collector specific heat capacity	$J.kg^{-1}.\ K^{-1}$	385.0	50
Negative current collector thermal conductivity	$W.m^{-1}.\ K^{-1}$	398.0	50
Negative current collector thickness	m	1.4e-05	49,50
Negative electrode density	kg/m^3	2242.0	50
Negative electrode specific heat capacity	$J.kg^{-1}.\ K^{-1}$	1437.4	50
Negative electrode thermal conductivity	$W.m^{-1}.\ K^{-1}$	1.04	50
Positive electrode thickness	m	4.5e-05	49
Positive electrode Bruggeman coefficient (electrolyte)	—	1.85	50
Positive electrode active material volume fraction ($\epsilon_{a,act}$)	—	0.808	50
Positive electrode porosity (ϵ_a)	—	0.178	50
Positive current collector density	kg/m^3	2710.0	50
Positive current collector specific heat capacity	$J.kg^{-1}.\ K^{-1}$	903.0	50
Positive current collector thermal conductivity	$W.m^{-1}.\ K^{-1}$	238.0	50
Positive current collector thickness	m	1.5e-05	49,50
Positive electrode density	kg/m^3	4870.0	50
Positive electrode specific heat capacity	$J.kg^{-1}.\ K^{-1}$	1269.21	50
Positive electrode thermal conductivity	$W.m^{-1}.\ K^{-1}$	1.58	50
Separator thickness	m	1.3e-05	49
Separator density	kg/m^3	1009.0	50
Separator specific heat capacity	$J.kg^{-1}K^{-1}$	1978.2	50
Separator thermal conductivity	$W.m^{-1}K^{-1}$	0.334 [50]	
Separator Bruggeman coefficient (electrolyte)	—	1.5	50
Separator porosity	—	0.40	b
Degradation related parameters considered as it is from "OKane2022" parameter set[52]			
Lithium plating kinetic rate constant	$m.\ s^{-1}$	1e-09	52
Lithium plating transfer coefficient	—	0.65	52
Dead lithium decay constant	s^{-1}	1e-06	52
Outer SEI solvent diffusivity	$m^2.\ s^{-1}$	2.50e-22	52
Negative electrode LAM constant proportional term	s^{-1}	2.7778e-07	52
Negative electrode LAM constant exponential term	—	2.0	52
Positive electrode LAM constant proportional term	s^{-1}	2.7778e-07	52
Positive electrode LAM constant exponential term	—	2.0	52

[a] The parameter values available in literature[48–52] were utilized. [b] Adjusted parameters.

Appendix B: Experimental Single Cell Data

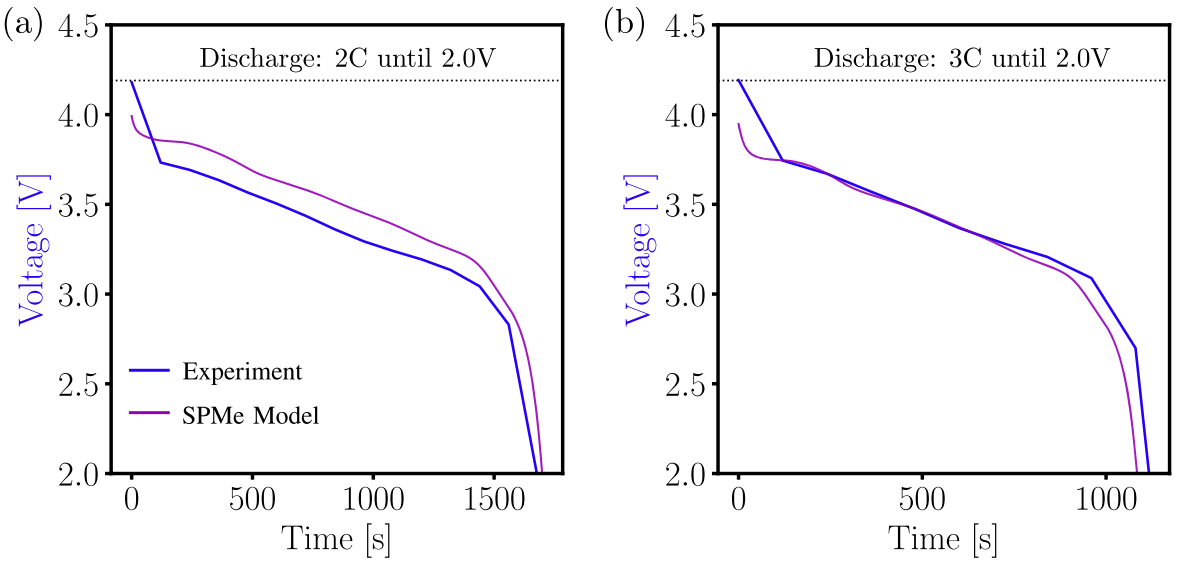

Figure B·1. Comparison of single cell simulations against experimental data. Inset (a) shows a 2C discharge where the simulation match experiments with an R^2 score of 0.89. Inset (b) shows a 3C discharge with simulations matching experiments with $R^2 = 0.92$.

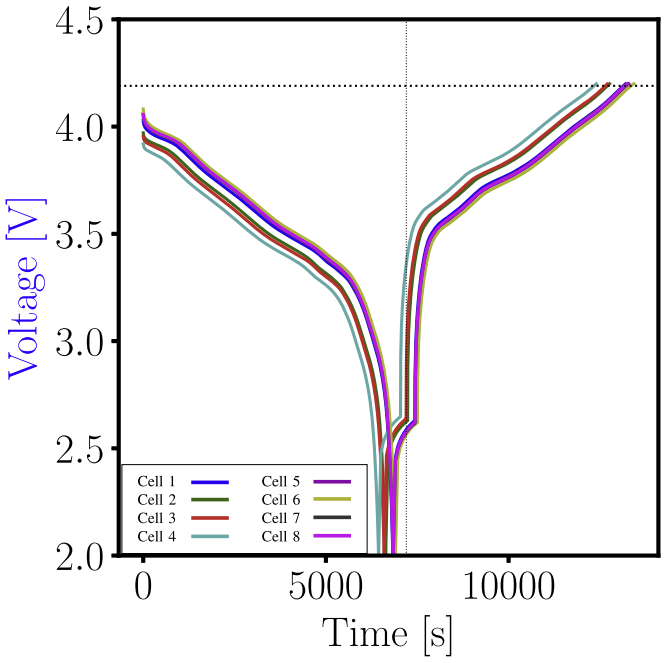

Figure B·2. Experimental cycling of individual cell before module tests. The voltage response of the 8 cells show slight differences when discharged at 0.5C, rested for 600 seconds, and charged at 0.5C, due to the variations in cell internal properties or cell aging. Thereby, each cell starts from a different initial electrode stoichiometries and initial capacities, which are supposed to be optimized for the models to replicate experimental findings.

Appendix C: Individual Cell Currents and Balancing

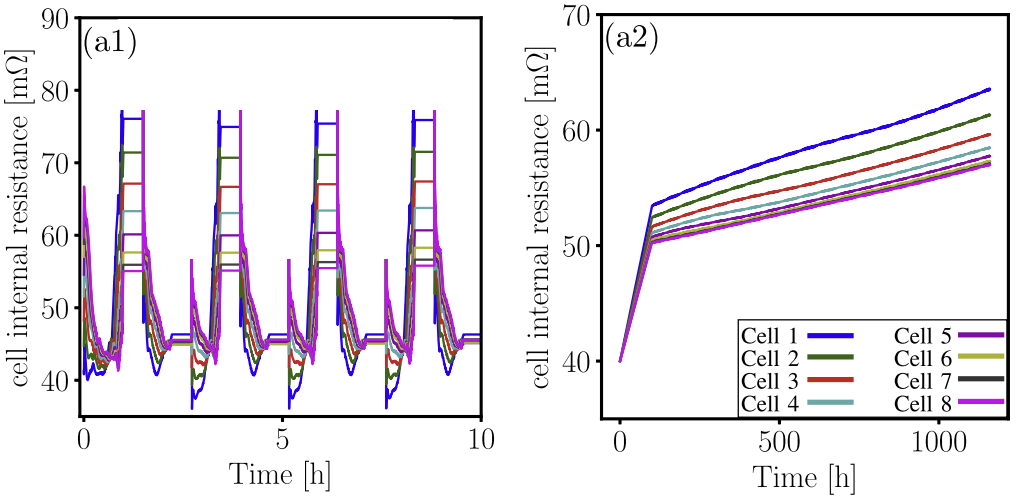

Figure C·1. Comparison of internal resistances of cells within the 8p1s module. The average trend of the internal resistances of the cells show a continuous increase in inset (a2), suggests the cell close to terminal experience increased degradation, and in long term could cause significant failure of the module. These trends in the internal resistance are subjected to change with the cycling conditions, degradation parameters and module circuit elements.

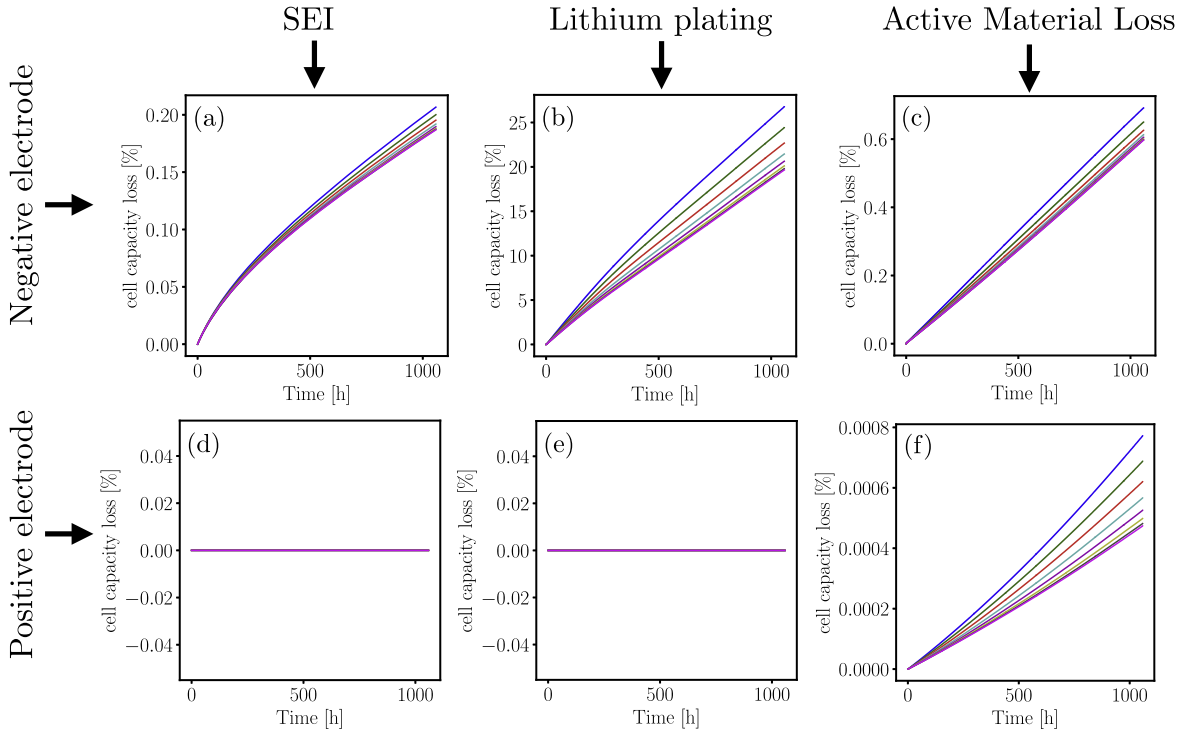

Figure C·2. Degradation contributions from different modes used within the model. Inset (b) shows that lithium plating is a major contributor to the overall degradation of the cells, this is due to the choice of the degradation parameters. Nevertheless, this highlights the frameworks capability to analyze the contributions of degradation modes at multiple scales, which are useful to develop aging informed BMS controls.

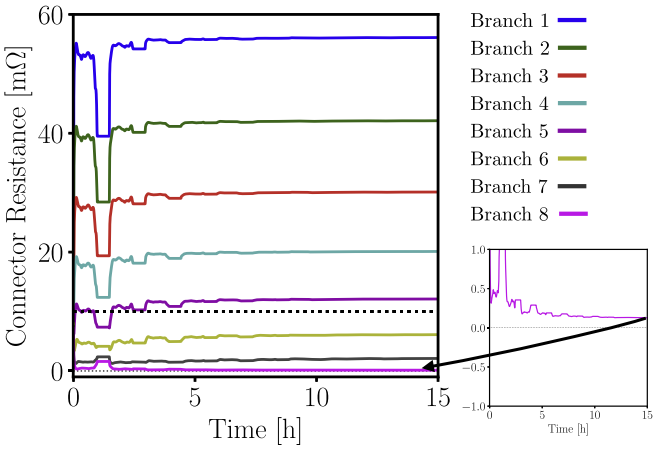

Figure C·3. The variable connector resistance during the active balancing. Despite the practicality, a non-uniform connector resistance in series could minimize imbalance by dissipating the excess energy from current imbalance.

Appendix D: Module Simulations at High C-rates

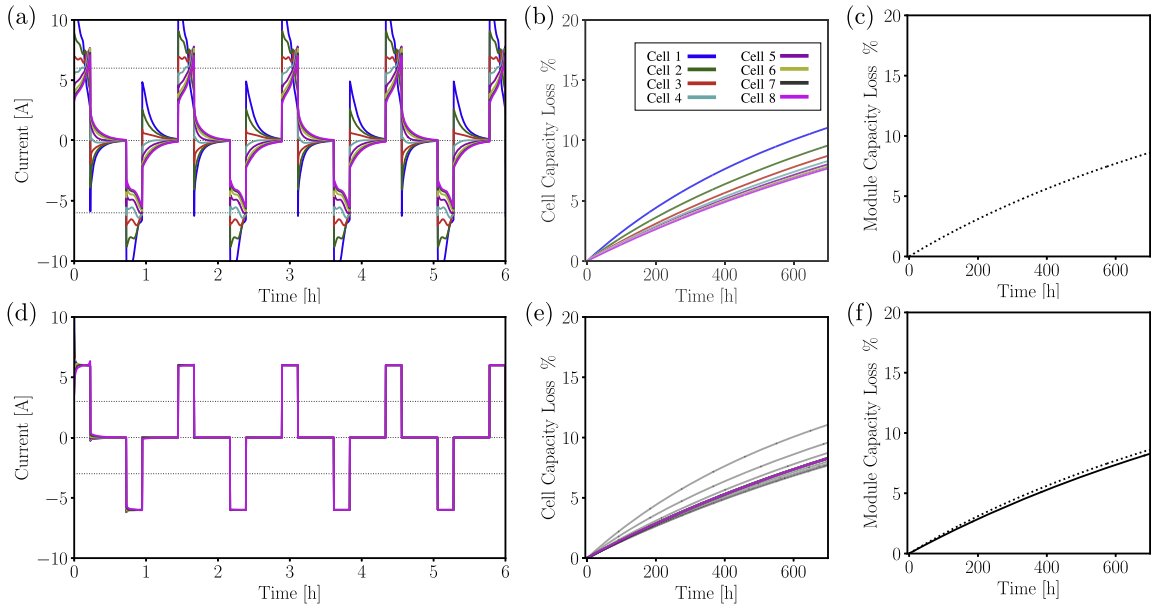

Figure D·1. 8p1s module cycling at 2C charge for 900 seconds followed by 30 minutes of rest, 2C discharge for 900 seconds followed by 30 minutes rest cycled for 500 cycles. Inset (a) shows the cell currents without any balancing. Inset (b) shows the individual cell capacity loss, inset (c) shows the overall module capacity loss. Inset (d) shows the cell currents with the cell active balancing. Inset (e) shows the individual cell capacity loss while the gray lines show the capacity loss without any active balancing. Inset (f) shows the comparison of overall module capacity loss with (solid line) and without (dotted line) active balancing , the module capacity improved by ∼5%. The results highlight that modules cycled at higher C-rate age faster due to higher current imbalances and increased heterogeneity in individual cell aging. Minimizing the current imbalances within the module improves the module life and aid with an easier aging analysis.

ORCID

Surya Mitra Ayalasomayajula https://orcid.org/0009-0008-6078-8713
Yuliya Preger https://orcid.org/0000-0001-8558-2529
Srikanth Allu https://orcid.org/0000-0003-2841-4398

References

1. H. C. Hesse, M. Schimpe, D. Kucevic, and A. Jossen, "Lithium-ion battery storage for the grid—a review of stationary battery storage system design tailored for applications in modern power grids." *Energies*, **10**, 2107 (2017).
2. G. Zubi, R. Dufo-López, M. Carvalho, and G. Pasaoglu, "The lithium-ion battery: state of the art and future perspectives." *Renew. Sustain. Energy Rev.*, **89**, 292 (2018).
3. D. Davies, M. Verde, O. Mnyshenko, Y. Chen, R. Rajeev, Y. Meng, and G. Elliott, "Combined economic and technological evaluation of battery energy storage for grid applications." *Nat. Energy*, **4**, 42 (2019).
4. C. Lu, H. Xu, X. Pan, and J. Song, "Optimal sizing and control of battery energy storage system for peak load shaving." *Energies*, **7**, 8396 (2014).
5. M. Rouholamini, C. Wang, H. Nehrir, X. Hu, Z. Hu, H. Aki, B. Zhao, Z. Miao, and K. Strunz, "A review of modeling, management, and applications of grid-connected li-ion battery storage systems." *IEEE Transactions on Smart Grid*, **13**, 4505 (2022).
6. S. M. Schoenung, *Energy storage systems cost update: a study for the DOE Energy Storage Systems Program.*, Sandia National Laboratories (SNL) (2011), , Technical Report.
7. M. T. Lawder, B. Suthar, P. W. Northrop, S. De, C. M. Hoff, O. Leitermann, M. L. Crow, S. Santhanagopalan, and V. R. Subramanian, "Battery energy storage system (bess) and battery management system (bms) for grid-scale applications." *Proc. IEEE*, **102**, 1014 (2014).

8. Z. Ma, M. Jia, L. Koltermann, A. Blömeke, R. W. De Doncker, W. Li, and D. U. Sauer, "Review on grid-tied modular battery energy storage systems: Configuration classifications, control advances, and performance evaluations." *Journal of Energy Storage*, **74**, 109272 (2023).
9. T. Chen, Y. Jin, H. Lv, A. Yang, M. Liu, B. Chen, Y. Xie, and Q. Chen, "Applications of lithium-ion batteries in grid-scale energy storage systems." *Transactions of Tianjin University*, **26**, 208 (2020).
10. T. Bruen and J. Marco, "Modelling and experimental evaluation of parallel connected lithium ion cells for an electric vehicle battery system." *Journal of Power Sources*, **310**, 91 (2016).
11. T. Weaver, A. Allam, and S. Onori, "A novel lithium-ion battery pack modeling framework-series-connected case study." *American Control Conference (ACC), IEEE*365 (2020).
12. X. Hu, C. Zou, C. Zhang, and Y. Li, "Technological developments in batteries: a survey of principal roles, types, and management needs." *IEEE Power and Energy Magazine*, **15**, 20 (2017).
13. K. Smith, G.-H. Kim, E. Darcy, and A. Pesaran, "Thermal/electrical modeling for abuse-tolerant design of lithium ion modules." *International Journal of Energy Research*, **34**, 204 (2010).
14. Z. Zhu, T. Jiang, M. Ali, Y. Meng, Y. Jin, Y. Cui, and W. Chen, "Rechargeable batteries for grid scale energy storage." *Chem. Rev.*, **122**, 16610 (2022).
15. K. Smith, A. Saxon, M. Keyser, B. Lundstrom, Z. Cao, and A. Roc, "Life prediction model for grid-connected li-ion battery energy storage system." *American Control Conference (ACC), IEEE*4062 (2017).
16. K. Moy, S. B. Lee, S. Harris, and S. Onori, "Design and validation of synthetic duty cycles for grid energy storage dispatch using lithium-ion batteries." *Advances in Applied Energy*, **4**, 100065 (2021).
17. M. Baumann, L. Wildfeuer, S. Rohr, and M. Lienkamp, "Parameter variations within li-ion battery packs–theoretical investigations and experimental quantification." *Journal of Energy Storage*, **18**, 295 (2018).
18. L. Chang, C. Ma, Y. Zhang, H. Li, and L. Xiao, "Experimental assessment of the discharge characteristics of multi-type retired lithium-ion batteries in parallel for echelon utilization." *Journal of Energy Storage*, **55**, 105539 (2022).
19. K. Rumpf, M. Naumann, and A. Jossen, "Experimental investigation of parametric cell-to-cell variation and correlation based on 1100 commercial lithium-ion cells." *Journal of Energy Storage*, **14**, 224 (2017).
20. R. Gogoana, M. B. Pinson, M. Z. Bazant, and S. E. Sarma, "Internal resistance matching for parallel-connected lithium-ion cells and impacts on battery pack cycle life." *Journal of Power Sources*, **252**, 8 (2014).
21. S. Miyatake, Y. Susuki, T. Hikihara, S. Itoh, and K. Tanaka, "Discharge characteristics of multicell lithium-ion battery with nonuniform cells." *Journal of Power Sources*, **241**, 736 (2013).
22. P. Jocher, M. Steinhardt, S. Ludwig, M. Schindler, J. Martin, and A. Jossen, "A novel measurement technique for parallel-connected lithium-ion cells with controllable interconnection resistance." *Journal of Power Sources*, **503**, 230030 (2021).
23. A. Fill, T. Mader, T. Schmidt, R. Llorente, and K. P. Birke, "Measuring test bench with adjustable thermal connection of cells to their neighbors and a new model approach for parallel-connected cells." *Batteries*, **6**, 2 (2019).
24. N. Yang, X. Zhang, B. Shang, and G. Li, "Unbalanced discharging and aging due to temperature differences among the cells in a lithium-ion battery pack with parallel combination." *Journal of Power Sources*, **306**, 733 (2016).
25. B. Wu, V. Yufit, M. Marinescu, G. J. Offer, R. F. Martinez-Botas, and N. P. Brandon, "Coupled thermal–electrochemical modelling of uneven heat generation in lithium-ion battery packs." *Journal of Power Sources*, **243**, 544 (2013).
26. M. Schindler, P. Jocher, A. Durdel, and A. Jossen, "Analyzing the aging behavior of lithium-ion cells connected in parallel considering varying charging profiles and initial cell-to-cell variations." *J. Electrochem. Soc.*, **168**, 090524 (2021).
27. Z. B. Omariba, L. Zhang, and D. Sun, "Review of battery cell balancing methodologies for optimizing battery pack performance in electric vehicles." *IEEE Access*, **7**, 129335 (2019).
28. S. Wen, "Cell balancing buys extra run time and battery life." *Analog Applications Journal*, **1**, 14–18 (2009).
29. M. Daowd, N. Omar, P. Van Den Bossche, and J. Van Mierlo, "Passive and active battery balancing comparison based on matlab simulation." *IEEE Vehicle Power and Propulsion Conference, IEEE*1 (2011).
30. F. Berger, D. Joest, E. Barbers, K. Quade, Z. Wu, D. U. Sauer, and P. Dechent, "Benchmarking battery management system algorithms-requirements, scenarios and validation for automotive applications." *eTransportation*, **22**, 100355 (2024).
31. M. Lelie, T. Braun, M. Knips, H. Nordmann, F. Ringbeck, H. Zappen, and D. U. Sauer, "Battery management system hardware concepts: an overview." *Applied Sciences*, **8**, 534 (2018).
32. X. Liu, W. Ai, M. N. Marlow, Y. Patel, and B. Wu, "The effect of cell-to-cell variations and thermal gradients on the performance and degradation of lithium-ion battery packs." *Applied Energy*, **248**, 489 (2019).
33. R. Luca, M. Whiteley, T. Neville, T. Tranter, J. Weaving, J. Marco, P. R. Shearing, and D. J. Brett, "Current imbalance in parallel battery strings measured using a hall-effect sensor array." *Energy Technology*, **9**, 2001014 (2021).
34. K. Rumpf, A. Rheinfeld, M. Schindler, J. Keil, T. Schua, and A. Jossen, "Influence of cell-to-cell variations on the inhomogeneity of lithium-ion battery modules." *J. Electrochem. Soc.*, **165**, A2587 (2018).
35. Y. Ren, K. Liu, T. Grandjean, W. D. Widanage, and J. Marco, "Current distribution and anode potential modelling in battery modules with a real-world busbar system." *IEEE Transactions on Transportation Electrification*, **9**, 4862 (2022).
36. G. Piombo, S. Fasolato, R. Heymer, M. Hidalgo, M. F. Niri, S. Onori, and J. Marco, "Unveiling the performance impact of module level features on parallel-connected lithium-ion cells via explainable machine learning techniques on a full factorial design of experiments." *Journal of Energy Storage*, **84**, 110783 (2024).
37. A. Reiter, S. Lehner, O. Bohlen, and D. U. Sauer, "Electrical cell-to-cell variations within large-scale battery systems—a novel characterization and modeling approach." *Journal of Energy Storage*, **57**, 106152 (2023).
38. J. M. Reniers and D. A. Howey, "Digital twin of a mwh-scale grid battery system for efficiency and degradation analysis." *Applied Energy*, **336**, 120774 (2023).
39. K. Kim and J.-I. Choi, "Effect of cell-to-cell variation and module configuration on the performance of lithium-ion battery systems." *Applied Energy*, **352**, 121888 (2023).
40. K. Vikrant, T. G. Tranter, G. M. Wiggins, D. J. Brett, and S. Allu, "Ageing studies of mega battery packs for grid storage applications using physics based modeling." *IEEE Electrical Energy Storage Application and Technologies Conference (EESAT), IEEE*1 (2024).
41. Y. Preger, J. Mueller, A. Fresquez, S. Allu, and C. Rich, "Impact of module configuration on lithium-ion battery performance and degradation: Part i. energy throughput, voltage spread, and current distribution." *J. Electrochem. Soc.*, **172**, 050540 (2025).
42. T. Tranter et al., "liionpack: a python package for simulating packs of batteries with pybamm." *Journal of Open Source Software*, **7**, 4051 (2022).
43. V. Sulzer, S. G. Marquis, R. Timms, M. Robinson, and S. J. Chapman, "Python battery mathematical modelling (pybamm)." *Journal of Open Research Software*, **9**, 14 (2021).
44. S. G. Marquis, V. Sulzer, R. Timms, C. P. Please, and S. J. Chapman, "An asymptotic derivation of a single particle model with electrolyte." *J. Electrochem. Soc.*, **166**, A3693 (2019).
45. V. Sulzer, S. G. Marquis, R. Timms, M. Robinson, and S. J. Chapman, (2025), https://docs.pybamm.org/en/stable/index.html Python Battery Mathematical Modelling (PyBaMM).
46. G. Brocard, *The LTspice IV Simulator: Manual, Methods and Applications* (Würth Elektronik) (2013).
47. C.-W. Ho, A. Ruehli, and P. Brennan, "The modified nodal approach to network analysis." *IEEE Transactions on Circuits and Systems*, **22**, 504 (1975).
48. C.-H. Chen, F. B. Planella, K. O'regan, D. Gastol, W. D. Widanage, and E. Kendrick, "Development of experimental techniques for parameterization of multi-scale lithium-ion battery models." *J. Electrochem. Soc.*, **167**, 080534 (2020).
49. T. T. D. Nguyen, "Understanding and modelling the thermal runaway of Li-ion batteries." *Ph.D. thesis, Université de Picardie Jules Verne* (2021).
50. B. J. Azuaje-Berbecí and H. B. Ertan, "A model for the prediction of thermal runaway in lithium–ion batteries." *Journal of Energy Storage*, **90**, 111831 (2024).
51. A. García, J. Monsalve-Serrano, A. Ponce-Mora, and Á. Fogué-Robles, "Development of a calibration methodology for fitting the response of a lithium-ion cell p2d model using real driving cycles." *Energy*, **271**, 126992 (2023).
52. S. E. O'Kane, W. Ai, G. Madabattula, D. Alonso-Alvarez, R. Timms, V. Sulzer, J. S. Edge, B. Wu, G. J. Offer, and M. Marinescu, "Lithium-ion battery degradation: how to model it." *Phys. Chem. Chem. Phys.*, **24**, 7909 (2022).
53. R. Wittman et al., "Characterization of cycle-aged commercial nmc and nca lithium-ion cells: I. temperature-dependent degradation." *J. Electrochem. Soc.*, **170**, 120538 (2023).
54. B. Planden, N. E. Courtier, M. Robinson, A. Khetarpal, F. B. Planella, and D. A. Howey, *arXiv* (2024), arXiv: 2412.15859 Pybop: a python package for battery model optimisation and parameterisation .
55. B. Planden, N. Courtier, and D. Howey, (2024), https://www.github.com/pybop-team/pybopPython Battery Optimisation and Parameterisation (PyBOP).
56. Y. Preger, H. M. Barkholtz, A. Fresquez, D. L. Campbell, B. W. Juba, J. Romàn-Kustas, S. R. Ferreira, and B. Chalamala, "Degradation of commercial lithium-ion cells as a function of chemistry and cycling conditions." *J. Electrochem. Soc.*, **167**, 120532 (2020).
57. "Battery Archive." (2024), https://batteryarchive.org/ Accessed: 2024-06-30.
58. Y. Preger, J. Mueller, G. Baker, and A. Fresquez, (2022), "(No. SAND2022-13742C), Sandia National Lab.(SNL-NM), Albuquerque, NM (United States), ECS Fall Meeting 2022 .
59. "Lithium Ion LG 18650 HG2 3000mAh Specifications" (2024) https://www.battery-space.com/prod-specs/9989.specs.pdf?srsltid=AfmBOoppKQZbHcczgLgk2zIU8RmPFT-PdI3zaTjWc9V1_-Cs1WNb8p_z Accessed: 2024-07-01.
60. A. Tomaszewska et al., "Lithium-ion battery fast charging: a review." *ETransportation*, **1**, 100011 (2019).